






Spin-lattice dynamics model with angular momentum transfer for canonical and microcanonical ensembles

Mara Strungaru ^{1,*}, Matthew O. A. Ellis ², Sergiu Ruta ¹, Oksana Chubykalo-Fesenko,³ Richard F. L. Evans ¹, and Roy W. Chantrell ¹

¹*Department of Physics, University of York, York YO10 5DD, United Kingdom*

²*Department of Computer Science, University of Sheffield, Sheffield S1 4DP, United Kingdom*

³*Instituto de Ciencia de Materiales de Madrid, CSIC, Madrid 28049, Spain*



(Received 1 October 2020; revised 22 December 2020; accepted 22 December 2020; published 19 January 2021)

A unified model of molecular and atomistic spin dynamics is presented enabling simulations both in microcanonical and canonical ensembles without the necessity of additional phenomenological spin damping. Transfer of energy and angular momentum between the lattice and the spin systems is achieved by a phenomenological coupling term representing the spin-orbit interaction. The characteristic spectra of the spin and phonon systems are analyzed for different coupling strength and temperatures. The spin spectral density shows magnon modes together with the uncorrelated noise induced by the coupling to the lattice. The effective damping parameter is investigated showing an increase with both coupling strength and temperature. The model paves the way to understanding magnetic relaxation processes beyond the phenomenological approach of the Gilbert damping and the dynamics of the energy transfer between lattice and spins.

DOI: [10.1103/PhysRevB.103.024429](https://doi.org/10.1103/PhysRevB.103.024429)

I. INTRODUCTION

With the emergent field of ultrafast magnetization dynamics [1] understanding the flow of energy and angular momentum between electrons, spins, and phonons is crucial for the interpretation of the wide range of observed phenomena [2–5]. For example, phonons strongly pumped in the THz regime by laser excitation can modulate the exchange field and manipulate the magnetization as shown for the magnetic insulator YIG [6] or in Gd [7]. The excitation of THz phonons leads to a magnetic response with the same frequency in Gd [7], proving the necessity of considering the dynamics of both lattice and spins. Phonon excitations can modulate both anisotropy and exchange which can successfully manipulate [8–10] or potentially switch the magnetization [11,12], ultimately leading to the development of low-dissipative memories.

Magnetization relaxation is typically modeled using the phenomenological description of damping proposed by Landau and Lifshitz [13] and later Gilbert [14], where the precessional equation of motion is augmented by a frictionlike term, resulting in the Landau-Lifshitz-Gilbert (LLG) equation. This represents the coupling of the magnetic modes (given primarily by the localized atomic spin) with the non-magnetic modes (lattice vibrations and electron orbits). The LLG equation and its generalizations can be deduced from the quantum-mechanical approaches assuming an equilibrium phonon bath and the weak coupling of the spin to the bath

degrees of freedom [15–17]. Thus, the standard approach works on the supposition that the timescales between the environmental degrees of freedom and the magnetic degrees of freedom are well separated and reducing the coupling between the magnetization and its environment to a single phenomenological damping parameter [18,19]. In reality, the lattice and magnetization dynamics have comparable timescales, where the interaction between the two subsystems represents a source of damping, hence the necessity of treating spin and lattice dynamics in a self-consistent way.

To investigate these phenomena, and aiming at predictive power for the design of competitive ultrafast magnetic nanodevices, advanced frameworks beyond conventional micromagnetics and atomistic spin dynamics [20] are needed [21]. A complete description of magnetic systems includes the interaction between several degrees of freedom, such as lattice, spins, and electrons, modeled in a self-consistent simulation framework. The characteristic relaxation timescales of electrons are much smaller (\approx fs) in comparison to spin and lattice (100 fs-ps), hence, magnetization relaxation processes can be described via coupled spin and lattice dynamics, termed spin-lattice dynamics (SLD) [22–29]. SLD models can be crucial in disentangling the interplay between these subsystems. Spin-lattice coupling has recently been studied via first-principles methods. Fransson *et al.* [30] demonstrated the possible symmetries of magnon-phonon coupling and the challenge of accurately calculating the phonon dispersion in magnetic materials, as these will be affected by the spin-lattice coupling. Also, Gennaro *et al.* [31] have combined first-principles methods with atomistic spin dynamics to introduce the effect of the phonons in the fixed-lattice magnetic simulations by employing exchange parameters calculated for

*Corresponding author: mss555@york.ac.uk

different relaxation of the lattice. In this work, however, we directly model in a self-consistent way, the dynamics of both phonons and spins and the spin-lattice coupling is treated phenomenologically similarly to [22,25–27,29], the coupling being able to efficiently exchange energy and angular momentum between the two subsystems.

SLD models have so far considered either microcanonical (NVE: constant particle number, volume, and energy) [27,28] or canonical (NVT: constant particle number, volume, and temperature) ensembles with two Langevin thermostats connected to both lattice and spin subsystems [23,32]. Damping due to spin-lattice interactions only within the canonical ensemble (NVT) has not yet been addressed, but is of interest in future modeling of magnetic insulators at finite temperature. Here, we introduce a SLD model capable of describing both ensembles. Specifically, our model (i) takes into account the transfer of angular momentum from spin to lattice and vice versa, (ii) works both in a microcanonical ensemble (constant energy) and in a canonical ensemble (constant temperature), (iii) allows a fixed Curie temperature of the system independent of the spin-lattice coupling strength, (iv) disables uniform translational motion of the system and additional constant energy drift, which can be produced by certain spin-lattice coupling forms. Furthermore, in this work, the characteristics of the induced spin-lattice noise, the magnon-phonon induced damping, and the equilibrium properties of the magnetic system has been systematically investigated.

Since many SLD models use body-centered-cubic (bcc) Fe due to its considerably large magnetoelastic coupling and for the necessity to include both lattice and spin degrees of freedom to capture the bcc-fcc-bcc phase transition at high temperatures [33], for the SLD model developed here we also use the parameters for this material. The aim of this work is not, however, to accurately reflect the structural properties of bcc Fe, but to rather understand the effect of phonon inclusion onto the spin dynamics. Hence, Fe potentials were used because of the mere facts that they are well studied in the literature and thus we could benchmark our results with others.

The paper is organized as follows. We start by describing the computational model of spin-lattice dynamics and the magnetic and mechanical energy terms used in this framework (Sec. II). We then explore the equilibrium properties of the system for both microcanonical and canonical simulations, proving that our model is able to efficiently transfer both energy and angular momentum between the spin and lattice degrees of freedom. In Sec. III we compute the equilibrium magnetization as function of temperature for both a dynamic and static lattice and we show that the order parameter is not dependent on the details of the thermostat used. In Sec. IV we analyze the autocorrelation functions and spectral characteristics of magnon, phonons, and the coupling term proving that the pseudodipolar coupling efficiently mediates the transfer of energy from spins to the lattice and vice versa. We then calculate the temperature and coupling dependence of the induced magnon-phonon damping and we conclude that the values agree well with damping measured in magnetic insulators, where the electronic contributions to the damping can be neglected (Sec. V).

TABLE I. Summary comparison of the SLD model developed here against other spin dynamics models.

Model	Lattice	Lattice thermostat	Spin thermostat	Intrinsic spin damping
SLD	Dynamic	On	Off	Phonon induced
ASD	Fixed	Off	On	Electronic mainly

II. COMPUTATIONAL MODEL

In order to model the effects of both lattice and spin dynamics in magnetic materials, an atomistic system is adopted with localized atomic magnetic moments at the atomic coordinates. Within this framework we solve $9N$ coupled equations corresponding to atomic magnetic moment (or spin) \mathbf{S} , atomic position \mathbf{r} , and velocity \mathbf{v} . The system has, however, $8N$ degrees of freedom, due to the constraint of the spin moving on a unit sphere. The model can be extended to $9N$ degrees of freedom by including longitudinal fluctuations [34]. We note that for the temperatures used for these simulations the contribution from longitudinal fluctuations is small, especially for bcc Fe, where the magnitude of the magnetic moments is similar between the paramagnetic and ferromagnetic states [35]. The lattice and the magnetic systems can directly interact with each other via the position- and spin-dependent Hamiltonians. The total Hamiltonian of the system consists of a lattice \mathcal{H}_{lat} and magnetic \mathcal{H}_{mag} parts:

$$\mathcal{H}_{tot} = \mathcal{H}_{lat} + \mathcal{H}_{mag}. \quad (1)$$

The lattice Hamiltonian includes the classical kinetic and pairwise interatomic potential energies:

$$\mathcal{H}_{lat} = \sum_i \frac{m_i \mathbf{v}_i^2}{2} + \frac{1}{2} \sum_{i,j} U(r_{ij}). \quad (2)$$

Our model considers a harmonic potential (HP) defined as

$$U(r_{ij}) = \begin{cases} V_0(r_{ij} - r_{ij}^0)^2 / a_0^2, & r_{ij} < r_c \\ 0, & r_{ij} > r_c \end{cases} \quad (3)$$

where V_0 has been parametrized for bcc Fe in [27] and $a_0 = 1 \text{ \AA}$ is a dimension scale factor. To be more specific we consider the equilibrium distances r_{ij}^0 corresponding to a symmetric bcc structure. The interaction cutoff is $r_c = 7.8 \text{ \AA}$. The parameters of the potential are given in Table II. The harmonic potential has been used for simplicity, however, it can lead to rather stiff lattice for a large interaction cutoff.

Another choice of the potential used in our model is an anharmonic Morse potential (MP) parametrized in [36] for bcc Fe and defined as

$$U(r_{ij}) = \begin{cases} D[e^{-2a(r_{ij}-r_0)} - 2e^{-a(r_{ij}-r_0)}], & r_{ij} < r_c \\ 0, & r_{ij} > r_c. \end{cases} \quad (4)$$

The Morse potential approximates well the experimental phonon dispersion observed experimentally for bcc Fe [37] as shown in [38]. The phonon spectra for the choices of potential used in this work are given in Sec. IV. Other nonlinear choices of potential can be calculated via, for example, the embedded

TABLE II. Parameters used in the spin-lattice model to simulate bcc Fe.

Quantity	Symbol	Value	Units
Exchange [23]	J_0	0.904	eV
	r_c	3.75	Å
Harmonic potential [27]	V_0	0.15	eV
	r_c	7.8	Å
Morse potential [36]	D	0.4174	eV
	a	1.3885	Å
	r_0	2.845	Å
	r_c	7.8	Å
Magnetic moment	μ_s	2.22	μ_B
Coupling constant	C	0.5	
Mass	m	55.845	u
Lattice constant	a	2.87	Å
Lattice damping	η	0.6	s^{-1}

atom method [39,40]. One challenge of the SLD models is the development of spin-dependent many-body potentials, which are crucial for studies of the mechanical phase transitions, deformations, and defects [41]. The potentials employed here are simplistic, but can approximate well the phonon spectra of bcc Fe (both for the case of the Morse potential and for a better parametrized harmonic potential). As we will see in the next sections, the magnon properties, such as damping, are not strongly influenced by the choice of potential. Hence, we have decided to remain with this simple pairwise implementation to investigate the magnetic properties.

The spin Hamiltonian (\mathcal{H}_{mag}) used in our simulations consists of contributions from the exchange interaction, Zeeman energy, and a spin-lattice coupling Hamiltonian, given by the pseudodipolar coupling term (\mathcal{H}_c), which we will describe later:

$$\mathcal{H}_{\text{mag}} = -\frac{1}{2} \sum_{i,j} J(r_{ij}) (\mathbf{S}_i \cdot \mathbf{S}_j) - \sum_i \mu_i \mathbf{S}_i \cdot \mathbf{H}_{\text{app}} + \mathcal{H}_c, \quad (5)$$

where μ_i is the magnetic moment of atom i , \mathbf{S}_i is a unit vector describing its spin direction, and \mathbf{H}_{app} is an external applied magnetic field. The exchange interactions used in our simulations depend on atomic separation $J(r_{ij})$. They were calculated from first-principles methods for bcc Fe by Ma *et al.* [23] and follow the dependence

$$J(r_{ij}) = J_0 \left(1 - \frac{r_{ij}}{r_c}\right)^3 \Theta(r_c - r_{ij}), \quad (6)$$

where r_c is the cutoff and $\Theta(r_c - r_{ij})$ is the Heaviside step function, which implies no exchange coupling between spins situated at larger distance than r_c .

Several previous SLD models suffered from the fact that they did not allow angular momentum transfer between lattice and spin systems [28]. This happened for magnetization dynamics in the absence of spin thermostat, governed by symmetric exchange only, due to total angular momentum conservation. Beaujouan *et al.* [22] has proposed a spin-pair anisotropy term in the form of a pseudodipolar interaction to couple the magnetization to the lattice dynamics and to enable, for the first time, the transfer of angular momentum within the spin-lattice dynamic framework. The spatial

dependence in the anisotropy term also allows the inclusion of magnetoelastic effects. Similarly, Perera *et al.* [26] proposed different local anisotropy terms to mimic the spin-orbit coupling phenomenon due to symmetry breaking of the local environment. The approach by Perera *et al.* [26] was successful in thermalizing the subsystems, however, single-site anisotropy spin terms with position-dependent coefficients as employed in [26] can induce an artificial collective translational motion of the sample while the system is magnetically saturated, due to the force $-\frac{\partial \mathcal{H}_{\text{tot}}}{\partial \mathbf{r}_i}$ proportional to spin orientation. To avoid large collective motion of the atoms in the magnetic saturated state, we consider a two-site coupling term, commonly known as the pseudodipolar coupling, described by

$$\mathcal{H}_c = - \sum_{i,j} f(r_{ij}) \left[(\mathbf{S}_i \cdot \hat{\mathbf{r}}_{ij})(\mathbf{S}_j \cdot \hat{\mathbf{r}}_{ij}) - \frac{1}{3} \mathbf{S}_i \cdot \mathbf{S}_j \right]. \quad (7)$$

The origin of this term still lies in the spin-orbit interaction, appearing from the dynamic crystal field that affects the electronic orbitals and spin states. This is a phenomenological term and its form comes naturally to express the coupling between two spins due to the changes in the lattice. Its biquadratic form and the exchange-like second term are necessary to avoid lattice translation in the saturated state. In reality, the coupling between phonons and magnons is material specific and should be derived on a more strict basis. However, the goal of our paper is not to investigate magnetoelastic properties of Fe, but to construct a reasonable model of coupled spin and lattice dynamics. Several models from the literature have been tested and this simplest term was sufficient to avoid artifacts in the spin or lattice dynamics. The pseudodipolar coupling has been employed previously in SLD simulations, first by Beaujouan *et al.* [22] and followed by more recent works [25,27]. It was initially proposed by Van Vleck [42] and Akhiezer [43] as an approximation of the more complex spin-orbit Hamiltonian and has the same structure of a dipolar interaction, however, with a distance dependence that falls off rapidly, hence, the name pseudodipolar interaction. The exchange-like term $-\frac{1}{3} \mathbf{S}_i \cdot \mathbf{S}_j$ is necessary in order to preserve the Curie temperature of the system under different coupling strengths and to ensure no net anisotropy when the atoms form a symmetric cubic lattice. For the mechanical forces, the exchange-like term eliminates the anisotropic force that leads to a nonphysical uniform translation of the system when the magnetic system is saturated. The magnitude of the interactions is assumed to decay as $f(\mathbf{r}_{ij}) = C J_0 (a_0/r_{ij})^4$ as presented in [27] with C taken as a constant, for simplicity measured relative to the exchange interactions and $a_0 = 1$ Å is a dimension scale factor. The constant C can be estimated from *ab initio* calculations [26], approximated from magnetoelastic coefficients [27], or can be chosen to match the relaxation times and damping values, as in this work. In Ref. [26] the coupling constants of 0.1 eV has been chosen, to be in the same order of magnitude as values found by first-principles calculations such as locally self-consistent multiple scattering (LSMS) [44]. The above LSMS calculations with the account of thermal vibrations were reported to give the energy fluctuations in the same order of magnitude as the mean energy itself, hence the difficulty to accurately estimate the coupling

energy. In Ref. [27], the coefficient C has been obtained by approximating the ratio between the pseudodipolar energy and exchange energy by the ratio between the magnetoelastic energy and thermal isotropic energy $k_B T_C$.

Since the total Hamiltonian now depends on the coupled spin and lattice degrees of freedom ($\mathbf{v}_i, \mathbf{r}_i, \mathbf{S}_i$), the following equations of motion (EOM) need to be solved concurrently to obtain the dynamics of our coupled system:

$$\frac{\partial \mathbf{r}_i}{\partial t} = \mathbf{v}_i, \quad (8)$$

$$\frac{\partial \mathbf{v}_i}{\partial t} = -\eta \mathbf{v}_i + \frac{\mathbf{F}_i}{m_i}, \quad (9)$$

$$\frac{\partial \mathbf{S}_i}{\partial t} = -\gamma \mathbf{S}_i \times \mathbf{H}_i, \quad (10)$$

$$\mathbf{F}_i = -\frac{\partial \mathcal{H}_{tot}}{\partial \mathbf{r}_i} + \mathbf{\Gamma}_i, \quad (11)$$

$$\mathbf{H}_i = -\frac{1}{\mu_S \mu_0} \frac{\partial \mathcal{H}_{tot}}{\partial \mathbf{S}_i}, \quad (12)$$

where \mathbf{F}_i and \mathbf{H}_i represent the effective force and field, $\mathbf{\Gamma}_i$ represents the fluctuation term (thermal force), and η represents the friction term that controls the dissipation of energy from the lattice into the external thermal reservoir. The strength of the fluctuation term can be calculated by converting the dissipation equations into a Fokker-Planck equation and then calculating the stationary solution. The thermal force has the form of a Gaussian noise:

$$\langle \Gamma_{i\alpha}(t) \rangle = 0, \quad (13)$$

$$\langle \Gamma_{i\alpha}(t) \Gamma_{j\beta}(t') \rangle = \frac{2\eta k_B T}{m_i} \delta_{\alpha\beta} \delta_{ij} \delta(t - t'). \quad (14)$$

To prove that the complete interacting many-body spin-lattice framework presented in here is in agreement with the fluctuation-dissipation theorem [45], we have followed the approach presented by Chubykalo *et al.* [46] based on the Onsager relations. Linearizing the equation of motion for spins, we find that the kinetic coefficients for the spin system are zero, due to the fact that the spin and internal field are thermodynamic conjugate variables. Hence, if the noise applied to the lattice obeys the fluctuation dissipation theory, the coupled system will obey it as well, due to the precessional form of the equation of motion for the spin.

We compare the SLD model presented here with other existing models that do not take into account the lattice degrees of freedom [atomistic spin dynamics (ASD)]. Particularly, in our case we assume a fixed lattice position. The summary of the comparison is presented in Table I. Atomistic spin dynamics simulations (ASD) [18,20,47,48] have been widely used to study finite-size effects, ultrafast magnetization dynamics, and numerous other magnetic phenomena. Here the intrinsic spin damping (the Gilbert damping α_G) is phenomenologically included. In our case, since the lattice is fixed it is assumed to come from electronic contributions. This phenomenological approach is typically used for metals, where the intrinsic damping is given by mainly electronic contributions [49–51]. Consequently, only $3N$ ($2N$ degrees of freedom) equations of motion per atom describing the spin

dynamics are used:

$$\frac{\partial \mathbf{S}_i}{\partial t} = -\frac{\gamma}{(1 + \alpha_G^2)} \mathbf{S}_i \times (\mathbf{H}_i + \alpha_G \mathbf{S}_i \times \mathbf{H}_i) \quad (15)$$

with an additional field coming from the coupling to the fixed lattice positions. The temperature effects are introduced in spin variables by means of a Langevin thermostat. The spin thermostat is modeled by augmenting the effective fields by a thermal stochastic field ($\mathbf{H}_i = \boldsymbol{\xi}_i - \partial \mathcal{H} / \partial \mathbf{S}_i$) and its properties also follow the fluctuation-dissipation theorem:

$$\langle \xi_{i\alpha}(t) \rangle = 0, \quad (16)$$

$$\langle \xi_{i\alpha}(t) \xi_{j\beta}(t') \rangle = \frac{2\alpha_G k_B T}{\gamma \mu_S} \delta_{\alpha\beta} \delta_{ij} \delta(t - t'). \quad (17)$$

The characteristics of the above presented models are summarized in Table I.

To integrate the coupled spin and lattice equations of motion we used a Suzuki-Trotter decomposition (STD) method [52] known for its numerical accuracy and stability. The scheme can integrate noncommuting operators, such as is the case of spin-lattice models and conserves the energy and space-phase volume. The conservation of energy is necessary when dealing with microcanonical simulations. Considering the generalized coordinate $\mathbf{X} = \{\mathbf{r}, \mathbf{v}, \mathbf{S}\}$ the equations of motion can be rewritten using the Liouville operators:

$$\frac{\partial \mathbf{X}}{\partial t} = \hat{L} \mathbf{X}(t) = (\hat{L}_r + \hat{L}_v + \hat{L}_S) \mathbf{X}(t). \quad (18)$$

The solution for the Liouville equation is $\mathbf{X}(t + \Delta t) = e^{L \Delta t} \mathbf{X}(t)$. Hence, following the form of this solution and applying a Suzuki-Trotter decomposition as in Tsai's work [53,54], we can write the solution as

$$\mathbf{X}(t + \Delta t) = e^{\hat{L}_S \frac{\Delta t}{2}} e^{\hat{L}_v \frac{\Delta t}{2}} e^{\hat{L}_r \Delta t} e^{\hat{L}_v \frac{\Delta t}{2}} e^{\hat{L}_S \frac{\Delta t}{2}} \mathbf{X}(t) + O(\Delta t^3), \quad (19)$$

where L_S, L_v, L_r are the Liouville operators for the spin, velocity, and position. This update can be abbreviated as $(\mathbf{s}, \mathbf{v}, \mathbf{r}, \mathbf{v}, \mathbf{s})$ update. The velocity and position are updated using a first-order update, however, the spin needs to be updated using a Cayley transform [55,56], due to the fact that the norm of each individual spin needs to be conserved. Thus, we have

$$e^{\hat{L}_v \Delta t} \mathbf{v}_i = \mathbf{v}_i + \frac{\Delta t}{m_i} \mathbf{F}_i, \quad (20)$$

$$e^{\hat{L}_r \Delta t} \mathbf{r}_i = \mathbf{r}_i + \Delta t \mathbf{v}_i, \quad (21)$$

$$e^{\hat{L}_S \Delta t} \mathbf{S}_i = \frac{\mathbf{S}_i + \Delta t \mathbf{H}_i \times \mathbf{S}_i + \frac{\Delta t^2}{2} [(\mathbf{H}_i \cdot \mathbf{S}_i) \mathbf{H}_i - \frac{1}{2} \mathbf{H}_i^2 \mathbf{S}_i]}{1 + \frac{1}{4} \Delta t^2 \mathbf{H}_i^2}. \quad (22)$$

The spin equations of motions depend directly on the neighboring spin orientations (through the effective field), hence, individual spins do not commute with each other. We need to further decompose the spin system $\hat{L}_S = \sum_i \hat{L}_{S_i}$. The following decomposition will be applied for the spin system:

$$e^{\hat{L}_S (\Delta t/2)} = e^{\hat{L}_{S_1} (\Delta t/4)} \dots e^{\hat{L}_{S_N} (\Delta t/2)} \dots e^{\hat{L}_{S_1} (\Delta t/4)} + O(\Delta t^3). \quad (23)$$

Tests of the accuracy of the integration have been performed by checking the conservation of energy within the

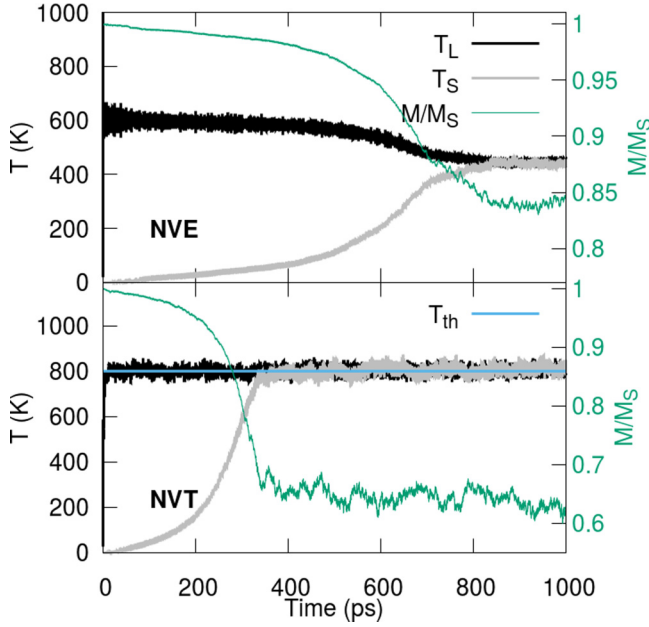


FIG. 1. NVE (top) and NVT (bottom) simulations for a $10 \times 10 \times 10$ unit-cell bcc Fe system. The spin system is initialized at $T_S = 0$ K corresponding to a saturated magnetic state in the z direction, while the lattice velocities are initialized by a Boltzmann distribution at $T_L = 1200$ K (for NVE) and $T_L = 600$ K (for NVT). In both cases we obtain equilibration of the two subsystems under 1 ns.

microcanonical ensemble. To ensure that the spin and lattice subsystems have reached equilibrium, we calculate both the lattice temperature (from the equipartition theorem) and spin temperature [57]. These are defined as

$$T_L = \frac{2}{3Nk_B} \sum_i \frac{\mathbf{p}_i^2}{2m}, \quad T_S = \frac{\sum_i (\mathbf{S}_i \times \mathbf{H}_i)^2}{2k_B \sum_i \mathbf{S}_i \cdot \mathbf{H}_i}. \quad (24)$$

III. SPIN-LATTICE THERMALIZATION

As an initial test of our model we look at the thermalization process within microcanonical (NVE) and canonical (NVT) simulations for a periodic bcc Fe system of $10 \times 10 \times 10$ unit cells. No thermostat is applied directly to the spin system and its thermalization occurs via transfer of energy and angular momentum from the lattice, i.e., via the magnon-phonon interaction. In the case of the NVE simulations, the energy is deposited into the lattice by randomly displacing the atoms from an equilibrium bcc structure positions within a 0.01 \AA radius sphere and by initializing their velocities with a Boltzmann distribution at $T = 1200$ K. The spin system is initialized on the z direction, corresponding to a spin temperature $T_S = 0$ K. In the case of NVT simulations, the lattice is connected to a thermostat at a temperature of $T = 800$ K. The parameters used in the simulations are presented in Table II.

Figure 1 shows the thermalization process for the two types of simulation. In both cases, the spin system has an initial temperature of $T_S = 0$ K corresponding to a saturated state in the z direction. For the NVE simulations, the two subsystems are seen to equilibrate at a temperature of $T = 445$ K, this temperature being dependent on the energy initially deposited

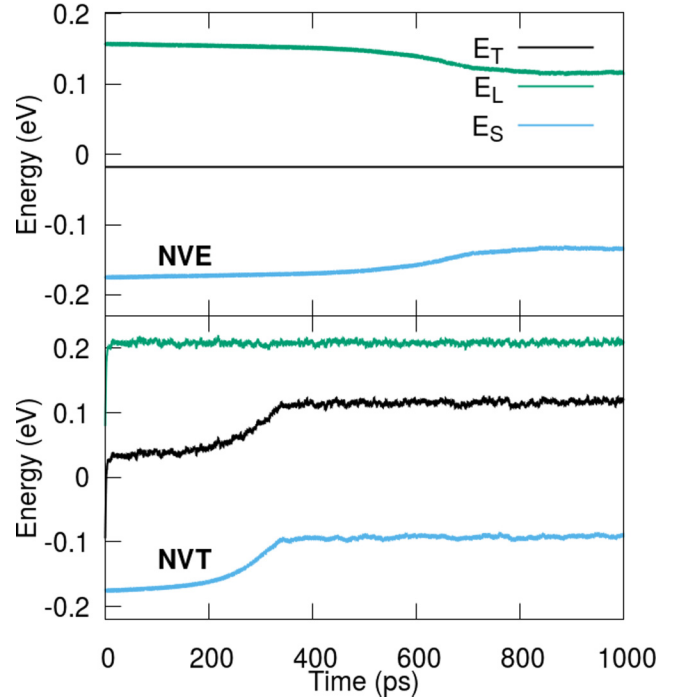


FIG. 2. Energies for NVE (top) and NVT (bottom) simulations for a $10 \times 10 \times 10$ unit-cell bcc Fe system corresponding to the simulations presented in Fig. 1.

into the system. In the NVT simulations, the lattice is thermalized at $T = 800$ K followed by the relaxation of the spin towards the same temperature. In both cases, we observe that the relaxation of the spin system happens under 1 ns, the relaxation timescale being dependent on the initial temperature of the subsystems. Since the spin subsystem is initialized at $T_S = 0$ K, the relaxation is slower, and overcomes the typical 100-ps values observed typically for spin-lattice relaxation. The corresponding change in the magnetization is emphasized by the green lines in Fig. 1 showing a transfer of angular momentum between the spin and lattice degrees of freedom. Figure 2 shows the variation of the total energy E_T , the lattice energy E_L , and spin energy E_S for both NVE and NVT simulations. The total energy is conserved for the NVE simulation and it is distributed between the lattice and spin degrees of freedom. For the NVT simulations, the total energy presents thermal fluctuations around a constant value, after an initial relaxation regime. We have also investigated the energy variation as function of the integration time step and concluded that an integration time step of $t_s = 0.5$ fs is sufficient to conserve the energy within the numerical precision of the simulations while keeping low computational cost.

To gain a better understanding of properties at thermal equilibrium within the spin-lattice dynamics model, we have investigated the temperature dependence of the magnetic order parameter in different frameworks that either enable or disable lattice dynamics, specifically, SLD or ASD. Table I illustrates the differences between the models. Since reaching joint thermal equilibrium depends strongly on the randomness already present in the magnetic system this process is accelerated by starting with a reduced magnetization of $M/M_S = 0.9$ for $T > 300$ K.

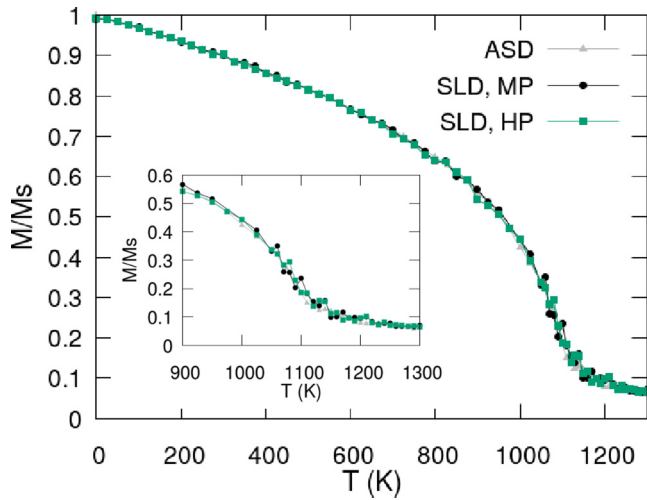


FIG. 3. Magnetization versus temperature curves for the SLD model (with different choices of lattice potential: MP, Morse potential; HP, harmonic potential), and fixed lattice ASD model. The inset zooms around the ferromagnetic to paramagnetic phase transition temperature.

Figure 3 shows the comparison of the equilibrium magnetization using either the harmonic potential (HP), Morse potential (MP), or fixed lattice (ASD) simulations. The magnetization is calculated by averaging for 200 ps after an initial equilibration for 800 ps (for SLD type simulations) or 100 ps (for ASD) simulations. We observe that even without a spin thermostat (in SLD model) the magnetization reaches equilibrium via the thermal fluctuations of the lattice, proving that both energy and angular momentum can be successfully transferred between the two subsystems. Additionally, both the SLD and ASD methods give the same equilibrium magnetization over the temperature range considered. This confirms that the equilibrium quantities are independent of the details of the thermostat used, in agreement with the fact that both SLD and ASD models obey the fluctuation-dissipation theorem.

In principle, since the strength of the exchange interaction depends on the relative separation between the atoms, any thermal expansion of the lattice could potentially modify the Curie temperature. However, as highlighted in the inset of Fig. 3, the same Curie temperature is observed in each model. We attribute this to fact that the thermal lattice expansion is small in the temperature range considered due to two reasons: (i) the Curie temperature of the system is well below the melting point of Fe (≈ 1800) K and (ii) we model a bulk, constant-volume system with periodic boundary conditions that does not present strong lattice displacements due to surfaces. We note that Evans *et al.* [58] found a reduction of T_C in nanoparticles due to an expansion of atomic separations at the surface that consequently reduces the exchange interactions. For systems with periodic boundary conditions we anticipate fluctuations in the exchange parameter due to changes in interatomic spacings to be relatively small. Our calculations of effective exchange constant for a dynamic lattice showed a variation of about 1% with respect to the static lattice, a difference that it is not reflected in the equilibrium magnetization curves. By removing the periodicity

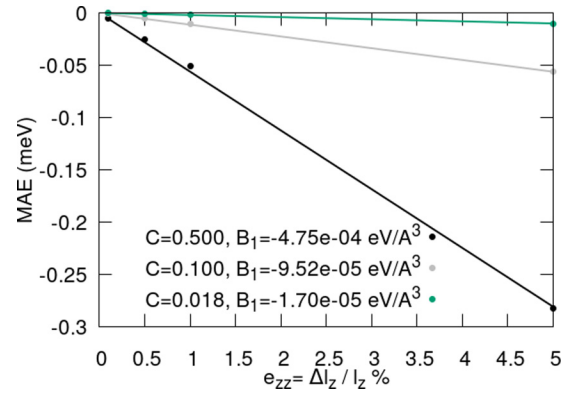


FIG. 4. Magnetic anisotropy energy as function of strain for different coupling strengths for $T = 0$ K.

of the system, different Curie temperatures can be observed between the static and dynamic lattice cases, due to the surface effects that induce a variation of the effective exchange constant in the order of 10%. Santos *et al.* [59] have performed a systematic comparison of the finite-size effects of the magnetization of static and dynamic lattice calculations and their results showed differences between the two even in the case of periodic systems. This suggests that the individual parametrization of the exchange and interatomic potential can largely influence the behavior of the equilibrium magnetization. Although, for the parametrization used in this work we show that the equilibrium properties are not dependent on the details of the thermostat or the potential, the magnetization dynamics could be strongly influenced by these choices.

The strength of the pseudodipolar coupling parameters C determines the timescale of the thermalization process. Its value can be parametrized from magnetoelastic simulations via calculations of the anisotropy energy as a function of strain. The magnetoelastic Hamiltonian can be written for a continuous magnetization \mathbf{M} and elastic strain tensor \mathbf{e} as [60,61]

$$\mathcal{H}_{m-e} = \frac{B_1}{M_S^2} \sum_i M_i^2 e_{ii} + \frac{B_2}{M_S^2} \sum_i M_i M_j e_{ij}, \quad (25)$$

where constants B_1, B_2 can be measured experimentally [62]. The pseudodipolar term acts as a local anisotropy, however, for a lattice distorted randomly, this effective anisotropy is averaged out to zero. At the same time, under external strain effects, an effective anisotropy will arise due to the pseudodipolar coupling which is the origin of the magnetoelastic effects. To calculate the induced magnetic anisotropy energy (MAE), the bcc lattice is strained along the z direction while fixed in the xy plane. The sample is then uniformly rotated and the energy barrier is evaluated from the angular dependence of the energy. Figure 4 shows MAE for different strain values and coupling strengths, with the magnetoelastic energy densities constants B_1 obtained from the linear fit. The values of the obtained constants B_1 are larger than the typical values reported for bcc Fe $B_1 = -3.43 \text{ MJ m}^{-3} = -2.14 \times 10^{-5} \text{ eV A}^{-3}$ [62] measured at $T = 300$ K which is similar to the B_1 value obtained for small coupling strengths $C = 0.018$. However, a larger coupling $C = 0.5$ is necessary in order to obtain damping parameters comparable to the ones known for

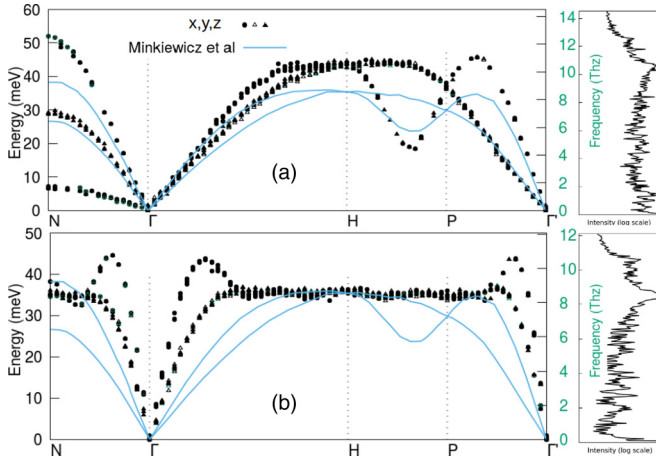


FIG. 5. Phonon spectra calculated for a $32 \times 32 \times 32$ unit-cell system at $T = 300$ K, $C = 0.5$ for (a) Morse potential, (b) harmonic potential. The spectra are calculated via method (i). Right figure includes the projection of the intensity of the spectra onto the frequency domain. Solid lines are the experimental data of Minkiewicz *et al.* [37]. For the Minkiewicz *et al.* data there is only one data point for the N - Γ path for the second transverse mode which does not show up on the line plots.

magnetic insulators where the main contribution comes from magnon-phonon scattering. In reality, in bcc Fe there is an important contribution to the effective damping from electronic sources, which, if considered, can lead to the smaller coupling strengths, consistent in magnitude with experimental magnetoelastic parameters. Indeed, as we will show later, our finding suggests that phonon damping is a very small contribution in metallic systems such as bcc Fe.

IV. DYNAMIC PROPERTIES AT THERMAL EQUILIBRIUM

Section III showed that the equilibrium magnetization does not depend on the details of the thermostat used and a successful transfer of both energy and angular momentum is achieved between the spin and lattice subsystems by the introduction of a pseudodipolar coupling term. In this section, we investigate the properties of the magnons, phonons, and the coupling term that equilibrates the spin and phonon systems in the absence of a phenomenological spin damping. Two types of simulations are presented here: (i) magnon and phonon spectra calculated along the high-symmetry path of a bcc lattice and (ii) averaged temporal Fourier transform (FT) of individual atom data sets (spin, velocity, pseudodipolar coupling field). The phonon (Fig. 5) and magnon (Fig. 6) spectra are calculated by initially equilibrating the system for 10 ps with a spin thermostat with $\alpha_G = 0.01$ and a coupling of $C = 0.5$, followed by 10 ps of equilibration in the absence of a spin thermostat. For the method (i) the correlations are computed for a runtime of 20 ps after the above thermalization stage. For each point in k space, the first three maxima of the autocorrelation function are plotted for better visualization. The autocorrelation function is projected onto the frequency space and the average intensity is plotted for different frequencies. The phonon spectra are calculated from the velocity autocorrelation function defined

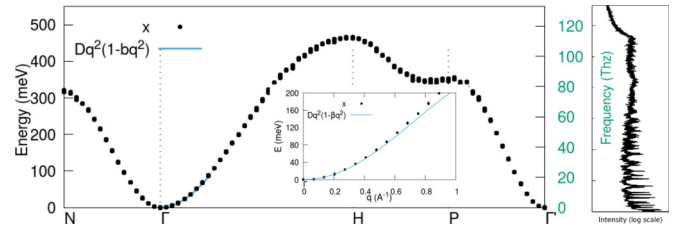


FIG. 6. Magnon spectrum (x component) calculated for a $32 \times 32 \times 32$ unit-cell system at $T = 300$ K, $C = 0.5$ for a Morse potential. The spectrum is calculated via method (i). The blue line is given by the dispersion equation $Dq^2(1 - \beta q^2)$, where the parameters $D = 307$ meV, $\beta = 0.32$ meV \AA^2 have been extracted from experimental measurements by Loong *et al.* [66]. The inset shows the behavior of the dispersion for low- q values. Right figure includes the projection of the intensity of the spectrum onto the frequency domain.

in Fourier space as [38,63]

$$A^p(k, \omega) = \int_0^{t_f} \langle v_k^p(t) v_k^p(t-t') \rangle e^{-i\omega t} dt, \quad (26)$$

where $p = x, y, z$, t_f is the total time, and $v_k^p(t)$ is the spatial Fourier transform calculated numerically as a discrete Fourier transform:

$$v_k^p(t) = \sum_i v_i^p e^{-ik \cdot r_i}. \quad (27)$$

The same approach is applied for the magnon spectra, using the dynamical spin structure factor, which is given by the space-time Fourier transform of the spin-spin correlation function defined as $C^{mn}(r-r', t-t') = \langle S^m(r, t) S^n(r', t') \rangle$, with m, n given by the x, y, z components [64]:

$$S^{mn}(\mathbf{k}, \omega) = \sum_{r, r'} e^{i\mathbf{k} \cdot (\mathbf{r} - \mathbf{r}')} \int_0^{t_f} C^{mn}(r-r', t-t') e^{-i\omega t} dt. \quad (28)$$

The second method (ii) to investigate the properties of the system involves calculating temporal Fourier transform of individual atom data sets, and averaging the Fourier response over 1000 atoms of the system. This response represents an integrated response over the k space. Hence, the projection of intensities on the frequency space presented by method (i) has similar features as the spectra presented by method (ii). For the results presented in Fig. 7, a system of $10 \times 10 \times 10$ bcc unit cells has been chosen. The system has been equilibrated for a total time of 20 ps with the method presented in (i) and the fast Fourier transform (FFT) is computed for the following 100 ps.

Figure 5 shows the phonon spectra for a SLD simulations at $T = 300$ K, $C = 0.5$ for the Morse potential [Fig. 5(a)] and the harmonic potential [Fig. 5(b)] calculated for the high-symmetry path of a bcc system with respect to both energy and frequency units. The interaction cutoff for both Morse and harmonic potentials is $r_c = 7.8$ \AA . The Morse phonon spectrum agrees well with the spectrum observed experimentally [37] and with the results from [38]. The projection of the spectra onto the frequency domain shows a peak close to 10.5 THz, due to the overlap of multiple phonon branches

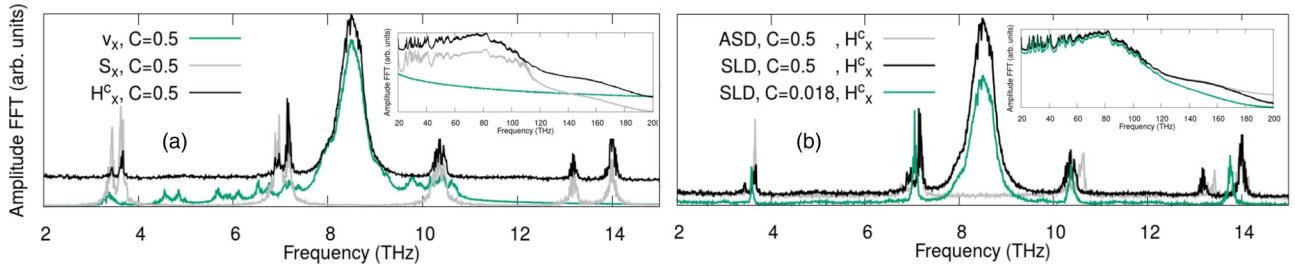


FIG. 7. The power spectral density of the autocorrelation function in the frequency domain for magnons, phonons, and coupling field for a SLD simulations with a harmonic lattice, calculated by method (ii). (a) Shows the power density of the autocorrelation function of the x component of the velocity v_x , spin S_x , and coupling field H_x^c . (b) Presents the power density of the autocorrelation function for the x component of the coupling field for either static (ASD) or dynamic (SLD) lattice. The insets show the high-frequency spectra. For (a) the velocity and the coupling field have been multiplied by a factor of 0.12 and 0.05, respectively, for easier graphical comparison.

at that frequency and consequently a large spectral density with many k points excited at this frequency. Moving now to the harmonic potential, parametrized as in Ref. [27], we first note that we observe that some of the phonon branches overlap [Fig. 5(b)]. Second, the projection of intensity onto the frequency domain shows a large peak at 8.6 THz, due to a flat region in the phonon spectra producing even larger number of k points in the spectrum which contribute to this frequency. Finally, the large cutoff makes the harmonic potential stiffer as all interactions are defined by the same energy V_0 and their equilibrium positions corresponding to a bcc structure. This is not the case for the Morse potential which depends exponentially on the difference between the interatomic distance and a constant equilibrium distance r_0 . For a long interaction range, the harmonic approximation will result in a more stiff lattice than the Morse parametrization.

In principle, the harmonic potential with a decreased interaction cutoff and an increased strength could better reproduce the full phonon spectra symmetry for bcc Fe. However, in this work we preferred to use the parametrization existing in literature [27] and a large interaction cutoff for stability purposes. Although the full symmetry of the bcc Fe phonon spectra is not reproduced by this harmonic potential, the phonon energies and frequencies are comparable to the values obtained with the Morse potential. Nevertheless, we observed the same equilibrium magnetization and damping (discussed later) for both potentials, hence, the simple harmonic potential represents a suitable approximation, that has the advantage of being more computationally efficient.

Figure 6 shows the magnon spectrum obtained within the SLD framework using the Morse potential together with its projection onto the frequency domain. The results agree very well with previous calculations of magnon spectra [28,65] and with the experimental magnon dispersion measured by Loong *et al.* [66]. For the comparison against experiments, we have used the analytical dispersion equation $Dq^2(1 - \beta q^2)$, where the parameters $D = 307$ meV, $\beta = 0.32$ meV \AA^2 have been extracted from experimental measurements. The inset of Fig. 6 shows the behavior of the dispersion for low- q values. For the harmonic potential the magnon spectrum is found to be identical to that for the Morse potential with only very small changes regarding the projection of intensity onto the frequency domain. This is in line with our discussion in the previous section where the choice of interatomic potential had

little effect on the Curie temperature, which is closely linked to the magnonic properties. As the harmonic potential is more computationally efficient than the Morse, we next analyze the properties of the system for a $10 \times 10 \times 10$ unit-cell system at $T = 300$ K with the harmonic potential.

The power spectral density (autocorrelation in Fourier space) of the magnon, phonons, and coupling field at 300 K is shown in Fig. 7 computed using method (ii) detailed previously. The amplitude of the FFT spectra of velocities and coupling field has been scaled by 0.12 and 0.05, respectively, to allow for an easier comparison between these quantities. As shown in Fig. 7(a) the coupling term presents both magnon and phonon characteristics, demonstrating an efficient coupling of the two subsystems. The large peak observed at a frequency of 8.6 THz appears as a consequence of the flat phonon spectrum for a harmonic potential, as observed in Fig. 5(b). Additionally, Fig. 7(a) can give us an insight into the induced spin noise within the SLD framework. The background of the FFT of the coupling field is flat for the frequencies plotted here, showing that the noise that acts on the spin is uncorrelated. The inset shows a larger frequency domain where it is clear that there are no phonon modes for these frequencies, and only thermal noise decaying with frequency is visible. At the same time, an excitation of spin modes is visible for frequencies up to about 100 THz.

The characteristics of the coupling field with respect to the coupling strength for a dynamic (SLD) and fixed lattice simulations (ASD) are presented in Fig. 7(b). The only difference between the ASD and SLD simulations is given by the presence of phonons (lattice fluctuations) in the latter. Since the large peak at 8.6 THz is due to the lattice vibrations, it is not present in the ASD simulations. The smaller peaks are present in both models since they are proper magnonic modes. With increasing coupling the width of the peaks increases, suggesting that the magnon-phonon damping has increased. Moving towards the larger frequency regimes [Fig. 7(b), inset], we observe that large coupling gives rise to a plateau in the spectra at around 150 THz, which is present as well for the fixed-lattice simulations (ASD). The plateau arises from a weak antiferromagnetic exchange that appears at large distances due to the competition between the ferromagnetic exchange and the antiferromagnetic exchange-like term in the pseudodipolar coupling.

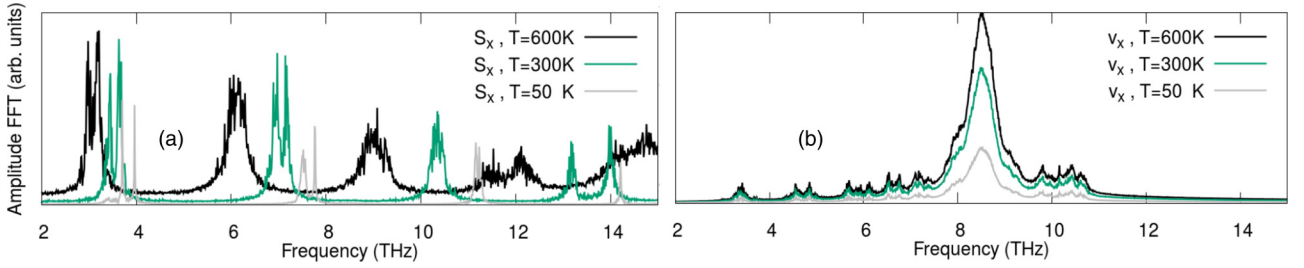


FIG. 8. The power spectral density of the autocorrelation function in the frequency domain for magnons (a) and phonons (b) for a SLD simulations with a harmonic lattice, calculated by method (ii), for three distinct temperatures and a coupling constant of $C = 0.5$.

We have also analyzed the characteristics of the magnon and phonon spectra for different temperatures (Fig. 8). With increasing temperature, the peaks corresponding to magnons shift to smaller frequencies. This is a typical situation known as a softening of low-frequency magnon modes due to the influence of thermal population (see, e.g., [67]) [Fig. 8(a)]. The same effect can be observed by calculating the magnon spectra via method (i) for various temperatures. In Fig. 8(b), the peak corresponding to phonons remains almost at the same frequency of about 8.6 THz, as the phonon spectra are not largely affected by temperatures up to $T = 600$ K. The increase of the effective damping (larger broadening) of each magnon mode with temperature is clearly observed.

V. MACROSCOPIC MAGNETIZATION DAMPING

In this section we evaluate the macroscopic damping parameter experienced by magnetization due to the magnon-phonon excitations for a periodic bcc system using our SLD model. This method for calculating the damping has been presented in [68–70]. The system is first thermalized at a nonzero temperature in an external field of $B_{ext} = 50$ T applied in the z direction, then the magnetization is rotated coherently through an angle of 30° . The system then relaxes back to equilibrium allowing the relaxation time to be extracted. The averaged z component of magnetization is then fitted to the function $m_z(t) = \tanh[\alpha\gamma B_{ext}(t + t_0)/(1 + \alpha^2)]$ where α represents the macroscopic (LLG-type) damping, γ the gyromagnetic ratio and t_0 a constant related to the initial conditions. The model system consists of $10 \times 10 \times 10$ unit cells and the damping value obtained from fitting of $m_z(t)$ is averaged over 10 different simulations.

Figure 9 shows the dependence of the average damping parameter together with the values obtained from individual simulations for different temperatures and coupling strengths for two choices of mechanical potential. In our model, the spin system is thermalized by the phonon thermostat, hence no electronic damping is present. With increasing coupling, the energy and angular momentum transfer is more efficient, hence the damping is enhanced. Since the observed value of induced damping is small, calculating the damping at higher temperature is challenging due to the strong thermal fluctuations that affect the accuracy of the results. Despite the low temperatures simulated here, the obtained damping values (at $T = 50$ K, $\alpha = 4.9 \times 10^{-5}$) are of the same order as reported for magnetic insulators such as YIG (1×10^{-4} to 1×10^{-6} [71,72]) as well as in different SLD simulations (3×10^{-5}

[27]). Generally, the induced damping value depends on the phonon characteristics and the coupling term, that allows transfer of both energy and angular momentum between the two subsystems.

Figures 9(a) and 9(b) compare the calculated damping for the Morse and harmonic potentials for two values of the coupling strength. We observe that the values are not greatly affected by the choice of potential. This arises due to the fact that only the spin modes around Γ point are excited and for these low k -vector modes the interatomic distances between neighboring atoms do not vary significantly. The extracted damping parameter as a function of coupling strength for 100 and 300 K is presented in Figs. 9(c) and 9(d), respectively. The functional form of the variation is quadratic, in accordance with the form of the coupling term. Measurements of damping in magnetic insulators, such as YIG, show a linear increase in the damping with temperature [72], which agrees with the relaxation rates calculated by Kasuya and LeCraw [73] and

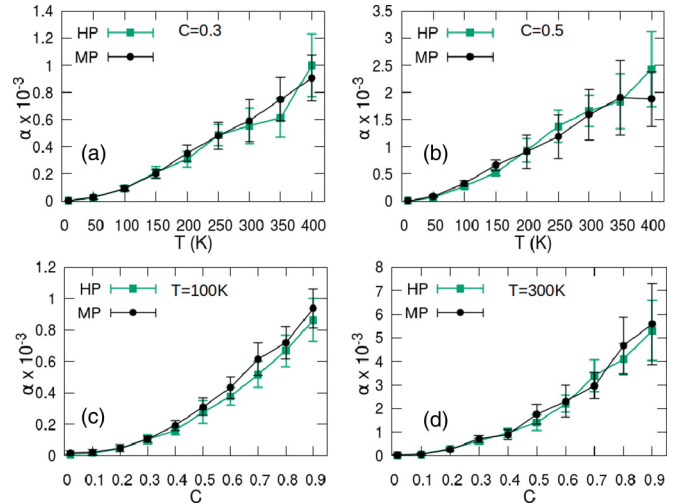


FIG. 9. Damping parameter extracted from fitting the z component of the magnetization for two different choices of potential: HP, harmonic potential (green open squares), and MP, Morse potential (black open circles), as function of temperature (a), (b) and as function of the coupling strength (c), (d). Panels (a) and (b) are calculated for a constant coupling strength of $C = 0.3$ and 0.5 , respectively. Panels (c) and (d) are calculated for temperatures of $T = 100$ and 300 K, respectively. The black and green lines represent the average damping parameter obtained from the simulations using the Morse and the harmonic potentials, respectively.

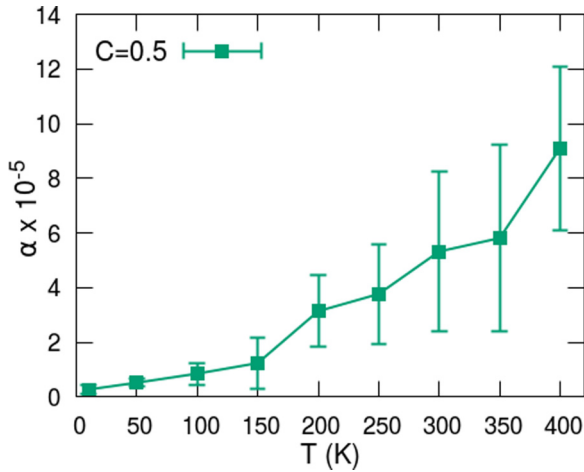


FIG. 10. Temperature variation of the damping parameter for Néel-type onsite coupling $H_c = -\sum_{i,j} f(r_{ij})[(\mathbf{S}_i \cdot \hat{\mathbf{r}}_{ij})^2 - \frac{1}{3}\mathbf{S}_i^2]$. The values are extracted from $m_z(t)$ fittings for 10 realizations.

the relaxation rates calculated in the NVE SLD simulations in Ref. [27]. However, Kasuya and LeCraw suggest that the relaxation rate can vary as T^n , where $n = 1 - 2$ with $n = 2$ corresponding to larger temperature regimes. Nevertheless, the difference between the quadratic temperature variation of the damping observed in our simulations and the linear one observed in experiments for YIG can be attributed to the difference in complexity between the bcc Fe model and YIG. The difference between the trends may as well suggest that the spin-orbit coupling in YIG could be described better by a linear phenomenological coupling term, such as the one used in Refs. [26,29], but we note that such forms can lead to a uniform force in the direction of the magnetization and so might need further adaptation before being suitable. To test an alternate form of the coupling we have replaced the pseudodipolar coupling to an onsite form, specifically $\mathcal{H}_c = -\sum_{i,j} f(r_{ij})[(\mathbf{S}_i \cdot \hat{\mathbf{r}}_{ij})^2 - \frac{1}{3}\mathbf{S}_i^2]$ i.e., a Néel-type anisotropy term. This is a test to understand the effect of the coupling term on the damping. The form of this coupling term leads to much smaller damping as shown in Fig. 10 ($T = 300$ K, $\alpha = 5.32 \times 10^{-5}$, averaged over 10 realizations) making it difficult to accurately calculate the temperature dependence of the damping, especially for large temperatures. The magnon-phonon damping can clearly have complex behavior depending on the properties of the system, especially the coupling term, hence no universal behavior of damping as function of temperature can be deduced for spin-lattice models.

Neglecting the lattice contribution, the temperature dependence of the macroscopic damping can be mapped onto the Landau-Lifshitz-Bloch formalism (LLB) [68] and theory [17] and ASD simulations [74] have shown it to vary inversely with the equilibrium magnetization. The LLB theory shows that the macroscopic damping is enhanced for large temperatures due to thermal spin fluctuations. Using the equilibrium magnetization it is possible to approximate the variation of damping with temperature produced due to thermal fluctuations within the LLB model. From 100 to 400 K the damping calculated via the LLB model increases within the order of 10^{-5} , which

is considerably smaller than the results obtained via the SLD model. This shows that within the SLD model the temperature increase of the damping parameter is predominantly due to magnon-phonon interaction, and not due to thermal magnon scattering, as this process is predominant at larger temperatures.

VI. CONCLUSIONS AND OUTLOOK

To summarize, we have developed a SLD model that is able to transfer energy and angular momentum efficiently from the spin to lattice subsystems and vice versa via a pseudodipolar coupling term. Our approach takes the best features from several previously suggested models and generalizes them which allows modeling in both canonical and microcanonical ensembles. With only the lattice coupled to a thermal reservoir and not the spin system, we reproduce the temperature dependence of the equilibrium magnetization, which agrees with the fact that the spin-lattice model obeys the fluctuation-dissipation theorem. We are able to study the dynamic properties such as phonon and spin spectrum and macroscopic damping, showing that the magnetic damping is not greatly influenced by the choice of potential, however, it is influenced by the form of the coupling term. This enables the possibility of tailoring the form of the coupling term so it can reproduce experimental dependencies of damping for different materials. We also find that the experimental magnetoelastic coupling B_1 can be reproduced by selecting the correct pseudodipolar coupling strength. In future, the addition of quantum statistics for spin-lattice dynamics models [75,76] may also yield better agreement with experimental data.

The SLD model developed here opens the possibility of the investigation of ultrafast dynamics experiments and theoretical studies of the mechanism through which angular momentum can be transferred from spin to the lattice at ultrafast timescales. As we have demonstrated that the model works well in the absence of a phenomenological Gilbert damping, which consists mainly of electronic contributions, the SLD model can be employed to study magnetic insulators, such as YIG, where the principal contribution to damping is via magnon-phonon interactions. Future application of this model includes controlling the magnetization via THz phonons [7] which can lead to nondissipative switching of the magnetization [11,12]. With the increased volume of data stored, field-free, heat-free switching of magnetic bits could represent the future of energy-efficient recording media applications. Another possible application is more advanced modeling of the ultrafast Einstein-de Haas effect [2] or phonon-spin transport [77].

ACKNOWLEDGMENTS

We are grateful to Dr. P.-W. Ma and Professor M. Probert for helpful discussions. Financial support of the Advanced Storage Research Consortium is gratefully acknowledged. M.O.A.E. gratefully acknowledges support in part from EP-SRC through Grant No. EP/S009647/1. The spin-lattice simulations were undertaken on the VIKING cluster, which is a high performance compute facility provided by the

University of York. The authors acknowledge the networking opportunities provided by the European COST Action

CA17123 “Magnetofon” and the short-time scientific mission awarded to M.S.

- [1] E. Beaurepaire, J.-C. Merle, A. Daunois, and J.-Y. Bigot, Ultrafast Spin Dynamics in Ferromagnetic Nickel, *Phys. Rev. Lett.* **76**, 4250 (1996).
- [2] C. Dornes, Y. Acremann, M. Savoini, M. Kubli, M. J. Neugebauer, E. Abreu, L. Huber, G. Lantz, C. A. F. Vaz, H. Lemke *et al.*, The ultrafast Einstein–de Haas effect, *Nature (London)* **565**, 209 (2019).
- [3] J. Walowski and M. Münzenberg, Perspective: Ultrafast magnetism and THz spintronics, *J. Appl. Phys.* **120**, 140901 (2016).
- [4] I. Radu, C. Stamm, A. Eschenlohr, F. Radu, R. Abrudan, K. Vahaplar, T. Kachel, N. Pontius, R. Mitzner, K. Hollmack *et al.*, Ultrafast and Distinct Spin Dynamics in Magnetic Alloys, *Spin* **5**, 1 (2015).
- [5] M. Hennecke, I. Radu, R. Abrudan, T. Kachel, K. Hollmack, R. Mitzner, A. Tsukamoto, and S. Eisebitt, Angular Momentum Flow During Ultrafast Demagnetization of a Ferrimagnet, *Phys. Rev. Lett.* **122**, 157202 (2019).
- [6] Sebastian F. Maehrlein, I. Radu, P. Maldonado, A. Paarmann, M. Gensch, Alexandra M. Kalashnikova, Roman V. Pisarev, M. Wolf, Peter M. Oppeneer, J. Barker, and T. Kampfrath, Dissecting spin-phonon equilibration in ferrimagnetic insulators by ultrafast lattice excitation, *Sci. Adv.* **4**, eaar5164 (2018).
- [7] A. Melnikov, I. Radu, U. Bovensiepen, O. Krupin, K. Starke, E. Matthias, and M. Wolf, Coherent Optical Phonons and Parametrically Coupled Magnons Induced by Femtosecond Laser Excitation of the *gd*(0001) Surface, *Phys. Rev. Lett.* **91**, 227403 (2003).
- [8] J.-W. Kim, M. Vomir, and J.-Y. Bigot, Controlling the spins angular momentum in ferromagnets with sequences of picosecond acoustic pulses, *Sci. Rep.* **5**, 8511 (2015).
- [9] J.-W. Kim, M. Vomir, and J.-Y. Bigot, Ultrafast Magnetoacoustics in Nickel Films, *Phys. Rev. Lett.* **109**, 166601 (2012).
- [10] A. V. Scherbakov, A. S. Salasyuk, A. V. Akimov, X. Liu, M. Bombeck, C. Bruggemann, D. R. Yakovlev, V. F. Sapega, J. K. Furdyna, and M. Bayer, Coherent Magnetization Precession in Ferromagnetic (ga,mn)as Induced by Picosecond Acoustic Pulses, *Phys. Rev. Lett.* **105**, 117204 (2010).
- [11] V. S. Vlasov, A. M. Lomonosov, A. V. Golov, L. N. Kotov, V. Besse, A. Alekhin, Dmitry A. Kuzmin, I. V. Bychkov, and V. V. Temnov, Magnetization switching in bistable nanomagnets by picosecond pulses of surface acoustic waves, *Phys. Rev. B* **101**, 024425 (2020).
- [12] O. Kovalenko, T. Pezeril, and V. V. Temnov, New Concept for Magnetization Switching by Ultrafast Acoustic Pulses, *Phys. Rev. Lett.* **110**, 266602 (2013).
- [13] L. D. Landau and E. M. Lifshitz, On the theory of the dispersion of magnetic permeability in ferromagnetic bodies, *Phys. Z. Sowjet.* **8**, 153 (1935).
- [14] T. L. Gilbert, A phenomenological theory of damping in ferromagnetic materials, *IEEE Trans. Magn.* **40**, 3443 (2004).
- [15] D. A. Garanin, Generalized equation of motion for a ferromagnet, *Phys. A (Amsterdam)* **172**, 470 (1991).
- [16] A. Rebei and G. J. Parker, Fluctuations and dissipation of coherent magnetization, *Phys. Rev. B* **67**, 104434 (2003).
- [17] P. Nieves, D. Serantes, U. Atxitia, and O. Chubykalo-Fesenko, Quantum Landau-Lifshitz-Bloch equation and its comparison with the classical case, *Phys. Rev. B* **90**, 104428 (2014).
- [18] M. O. A. Ellis, R. F. L. Evans, T. A. Ostler, J. Barker, U. Atxitia, O. Chubykalo-Fesenko, and R. W. Chantrell, The Landau-Lifshitz equation in atomistic models, *Low Temp. Phys.* **41**, 705 (2015).
- [19] S. Bhattacharjee, L. Nordstrom, and J. Fransson, Atomistic Spin Dynamic Method with both Damping and Moment of Inertia Effects Included from First Principles, *Phys. Rev. Lett.* **108**, 057204 (2012).
- [20] R. F. L. Evans, W. J. Fan, P. Chureemart, T. A. Ostler, M. O. A. Ellis, and R. W. Chantrell, Atomistic spin model simulations of magnetic nanomaterials, *J. Phys.: Condens. Matter* **26**, 103202 (2014).
- [21] B. Dieny, I. L. Prejbeanu, K. Garello, P. Gambardella, P. Freitas, R. Lehdorff, W. Raberg, U. Ebels, S. O. Demokritov, J. Akerman *et al.*, Opportunities and challenges for spintronics in the microelectronics industry, *Nat. Electron.* **3**, 446 (2020).
- [22] D. Beaujouan, P. Thibaudeau, and C. Barreateau, Anisotropic magnetic molecular dynamics of cobalt nanowires, *Phys. Rev. B* **86**, 174409 (2012).
- [23] P.-W. Ma, C. H. Woo, and S. L. Dudarev, Large-scale simulation of the spin-lattice dynamics in ferromagnetic iron, *Phys. Rev. B* **78**, 024434 (2008).
- [24] P.-W. Ma and C. H. Woo, Parallel algorithm for spin and spin-lattice dynamics simulations, *Phys. Rev. E* **79**, 046703 (2009).
- [25] J. Tranchida, S. J. Plimpton, P. Thibaudeau, and A. P. Thompson, Massively parallel symplectic algorithm for coupled magnetic spin dynamics and molecular dynamics, *J. Comput. Phys.* **372**, 406 (2018).
- [26] D. Perera, M. Eisenbach, D. M. Nicholson, G. M. Stocks, and D. P. Landau, Reinventing atomistic magnetic simulations with spin-orbit coupling, *Phys. Rev. B* **93**, 060402(R) (2016).
- [27] M. Aßmann and U. Nowak, Spin-lattice relaxation beyond Gilbert damping, *J. Magn. Magn. Mater.* **469**, 217 (2019).
- [28] J. Hellsvik, D. Thonig, K. Modin, D. Iusan, A. Bergman, O. Eriksson, L. Bergqvist, and A. Delin, General method for atomistic spin-lattice dynamics with first-principles accuracy, *Phys. Rev. B* **99**, 104302 (2019).
- [29] S. Karakurt, R. W. Chantrell, and U. Nowak, A model of damping due to spin-lattice interaction, *J. Magn. Magn. Mater.* **316**, e280 (2007).
- [30] J. Fransson, D. Thonig, P. F. Bessarab, S. Bhattacharjee, J. Hellsvik, and L. Nordstrom, Microscopic theory for coupled atomistic magnetization and lattice dynamics, *Phys. Rev. Mater.* **1**, 074404 (2017).
- [31] M. Di Gennaro, A. L. Miranda, T. A. Ostler, A. H. Romero, and M. J. Verstraete, Competition of lattice and spin excitations in the temperature dependence of spin-wave properties, *Phys. Rev. B* **97**, 214417 (2018).
- [32] P.-W. Ma, S. L. Dudarev, and C. H. Woo, Spin-lattice-electron dynamics simulations of magnetic materials, *Phys. Rev. B* **85**, 184301 (2012).

- [33] P.-W. Ma, S. L. Dudarev, and J. S. Wróbel, Dynamic simulation of structural phase transitions in magnetic iron, *Phys. Rev. B* **96**, 094418 (2017).
- [34] P.-W. Ma and S. L. Dudarev, Longitudinal magnetic fluctuations in langevin spin dynamics, *Phys. Rev. B* **86**, 054416 (2012).
- [35] A. V. Ruban, S. Khmelevskiy, P. Mohn, and B. Johansson, Temperature-induced longitudinal spin fluctuations in Fe and Ni, *Phys. Rev. B* **75**, 054402 (2007).
- [36] L. A. Girifalco and V. G. Weizer, Application of the Morse potential function to cubic metals, *Phys. Rev.* **114**, 687 (1959).
- [37] V. J. Minkiewicz, G. Shirane, and R. Nathans, Phonon dispersion relation for iron, *Phys. Rev.* **162**, 528 (1967).
- [38] M. Ellis, Simulations of magnetic reversal properties in granular recording media, Ph.D. thesis, University of York, 2015.
- [39] S. L. Dudarev and P. M. Derlet, A ‘magnetic’ interatomic potential for molecular dynamics simulations, *J. Phys.: Condens. Matter* **17**, 7097 (2005).
- [40] P. M. Derlet and S. L. Dudarev, Million-atom molecular dynamics simulations of magnetic iron, *Prog. Mater. Sci.* **52**, 299 (2007).
- [41] P.-W. Ma and S. L. Dudarev, “Atomistic spin-lattice dynamics,” in *Handbook of Materials Modeling: Methods: Theory and Modeling*, edited by Wanda Andreoni and Sidney Yip (Springer, Cham, 2020), pp. 1017–1035.
- [42] J. H. Van Vleck, On the anisotropy of cubic ferromagnetic crystals, *Phys. Rev.* **52**, 1178 (1937).
- [43] A. I. Akhiezer, S. V. Peletminskii, and V. G. Baryakhtar, *Spin waves*, (North-Holland Pub. Co., 1968).
- [44] M. Eisenbach, D. M. Nicholson, A. Rusanu, and G. Brown, First principles calculation of finite temperature magnetism in Fe and Fe₃C, *J. Appl. Phys.* **109**, 07E138 (2011).
- [45] R. Kubo, The fluctuation-dissipation theorem, *Rep. Prog. Phys.* **29**, 255 (1966).
- [46] O. Chubykalo, R. Smirnov-Rueda, J. M. Gonzalez, M. A. Wongsam, R. W. Chantrell, and U. Nowak, Brownian dynamics approach to interacting magnetic moments, *J. Magn. Magn. Mater.* **266**, 28 (2003).
- [47] O. Eriksson, A. Bergman, L. Bergqvist, and J. Hellsvik, *Atomistic Spin Dynamics: Foundations and Applications* (Oxford University Press, Oxford, 2017).
- [48] G. P. Muller, M. Hoffmann, C. Disselkamp, D. Schurhoff, S. Mavros, M. Sallermann, N. S. Kiselev, H. Jonsson, and S. Blugel, Spirit: Multifunctional framework for atomistic spin simulations, *Phys. Rev. B* **99**, 224414 (2019).
- [49] F. Kormann, B. Grabowski, B. Dutta, T. Hickel, L. Mauger, B. Fultz, and J. Neugebauer, Temperature Dependent Magnon-Phonon Coupling in bcc Fe from Theory and Experiment, *Phys. Rev. Lett.* **113**, 165503 (2014).
- [50] B. Dutta, F. Kormann, S. Ghosh, B. Sanyal, J. Neugebauer, and T. Hickel, Phonons in magnetically disordered materials: Magnetic versus phononic time scales, *Phys. Rev. B* **101**, 094201 (2020).
- [51] M. Heine, O. Hellman, and D. Broido, Effect of thermal lattice and magnetic disorder on phonons in bcc Fe: A first-principles study, *Phys. Rev. B* **100**, 104304 (2019).
- [52] M. Suzuki, Generalized Trotter’s formula and systematic approximations of exponential operators and inner derivations with applications to many-body problems, *Commun. Math. Phys.* **51**, 183 (1976).
- [53] S.-H. Tsai, H. K. Lee, and D. P. Landau, Molecular and spin dynamics simulations using modern integration methods, *Am. J. Phys.* **73**, 615 (2005).
- [54] S.-H. Tsai, M. Krech, and D. P. Landau, Symplectic integration methods in molecular and spin dynamics simulations, *Braz. J. Phys.* **34**, 384 (2004).
- [55] I. P. Omelyan, I. M. Mryglod, and R. Folk, Algorithm for Molecular Dynamics Simulations of spin Liquids, *Phys. Rev. Lett.* **86**, 898 (2001).
- [56] D. Lewis and N. Nigam, Geometric integration on spheres and some interesting applications, *J. Comput. Appl. Math.* **151**, 141 (2003).
- [57] P.-W. Ma, S. L. Dudarev, A. A. Semenov, and C. H. Woo, Temperature for a dynamic spin ensemble, *Phys. Rev. E* **82**, 031111 (2010).
- [58] R. Evans, U. Nowak, F. Dorfbauer, T. Shreffl, O. Mryasov, R. W. Chantrell, and G. Grochola, The influence of shape and structure on the Curie temperature of Fe and Co nanoparticles, *J. Appl. Phys.* **99**, 08G703 (2006).
- [59] G. Dos Santos, R. Aparicio, D. Linares, E. N. Miranda, J. Tranchida, G. M. Pastor, and E. M. Bringa, Size- and temperature-dependent magnetization of iron nanoclusters, *Phys. Rev. B* **102**, 184426 (2020).
- [60] C. Kittel, Physical theory of ferromagnetic domains, *Rev. Mod. Phys.* **21**, 541 (1949).
- [61] A. Kamra, H. Keshtgar, P. Yan, and G. E. W. Bauer, Coherent elastic excitation of spin waves, *Phys. Rev. B* **91**, 104409 (2015).
- [62] D. Sander, The correlation between mechanical stress and magnetic anisotropy in ultrathin films, *Rep. Prog. Phys.* **62**, 809 (1999).
- [63] N. I. Papanicolaou, I. E. Lagaris, and G. A. Evangelakis, Modification of phonon spectral densities of the (001) copper surface due to copper adatoms by molecular dynamics simulation, *Surf. Sci.* **337**, L819 (1995).
- [64] M. Krech, A. Bunker, and D. P. Landau, Fast spin dynamics algorithms for classical spin systems, *Comput. Phys. Commun.* **111**, 1 (1998).
- [65] D. Perera, D. M. Nicholson, M. Eisenbach, G. M. Stocks, and D. P. Landau, Collective dynamics in atomistic models with coupled translational and spin degrees of freedom, *Phys. Rev. B* **95**, 014431 (2017).
- [66] C.-K. Loong, J. M. Carpenter, J. W. Lynn, R. A. Robinson, and H. A. Mook, Neutron scattering study of the magnetic excitations in ferromagnetic iron at high energy transfers, *J. Appl. Phys.* **55**, 1895 (1984).
- [67] U. Atxitia, D. Hinzke, O. Chubykalo-Fesenko, U. Nowak, H. Kachkachi, O. N. Mryasov, R. F. Evans, and R. W. Chantrell, Multiscale modeling of magnetic materials: Temperature dependence of the exchange stiffness, *Phys. Rev. B* **82**, 134440 (2010).
- [68] O. Chubykalo-Fesenko, U. Nowak, R. W. Chantrell, and D. Garanin, Dynamic approach for micromagnetics close to the curie temperature, *Phys. Rev. B* **74**, 094436 (2006).
- [69] M. O. A. Ellis, T. A. Ostler, and R. W. Chantrell, Classical spin model of the relaxation dynamics of rare-earth doped permalloy, *Phys. Rev. B* **86**, 174418 (2012).

- [70] M. Strungaru, S. Ruta, R. F. L. Evans, and R. W. Chantrell, Model of magnetic damping and anisotropy at elevated temperatures: Application to granular FePt films, *Phys. Rev. Applied* **14**, 014077 (2020).
- [71] C. L. Jermain, S. V. Aradhya, N. D. Reynolds, R. A. Buhrman, J. T. Brangham, M. R. Page, P. C. Hammel, F. Y. Yang, and D. C. Ralph, Increased low-temperature damping in yttrium iron garnet thin films, *Phys. Rev. B* **95**, 174411 (2017).
- [72] H. Maier-Flaig, S. Klingler, C. Dubs, O. Surzhenko, R. Gross, M. Weiler, H. Huebl, and S. T. B. Goennenwein, Temperature-dependent magnetic damping of yttrium iron garnet spheres, *Phys. Rev. B* **95**, 214423 (2017).
- [73] T. Kasuya and R. C. LeCraw, Relaxation Mechanisms in Ferromagnetic Resonance, *Phys. Rev. Lett.* **6**, 223 (1961).
- [74] M. O. A. Ellis, M. Galante, and S. Sanvito, Role of longitudinal fluctuations in L10 FePt, *Phys. Rev. B* **100**, 214434 (2019).
- [75] R. F. L. Evans, U. Atxitia, and R. W. Chantrell, Quantitative simulation of temperature-dependent magnetization dynamics and equilibrium properties of elemental ferromagnets, *Phys. Rev. B* **91**, 144425 (2015).
- [76] J. Barker and G. E. W. Bauer, Semiquantum thermodynamics of complex ferrimagnets, *Phys. Rev. B* **100**, 140401(R) (2019).
- [77] A. Ruckriegel and R. A. Duine, Long-Range Phonon Spin Transport in Ferromagnet–Nonmagnetic Insulator Heterostructures, *Phys. Rev. Lett.* **124**, 117201 (2020).